The Journal of Chemical Physics

RESEARCH ARTICLE | JUNE 24 2026

Microscopic origin of droplet line tension

Franziska Aurbach ; Fei Wang ; Britta Nestler

J. Chem. Phys. 164, 244702 (2026)
https://doi.org/10.1063/5.0332465

The Journal of Chemical Physics ARTICLE pubs.aip.org/aip/jcp

Microscopic origin of droplet line tension

Cite as: J. Chem. Phys. 164, 244702 (2026); doi: 10.1063/5.0332465
Submitted: 4 March 2026 • Accepted: 8 June 2026 •
Published Online: 24 June 2026

Franziska Aurbach,[1,2] Fei Wang,[1,2,a)] and Britta Nestler[1,2,3]

AFFILIATIONS

[1] Institute of Applied Materials-Microstructure Modelling and Simulation, Karlsruhe Institute of Technology, Straße Am Forum 7, Karlsruhe 76131, Germany
[2] Institute of Nanotechnology, Karlsruhe Institute of Technology, Hermann-von-Helmholtz-Platz 1, Eggenstein-Leopoldshafen 76344, Germany
[3] Institute of Digital Materials Science, Karlsruhe University of Applied Sciences, Moltkestraße 30, Karlsruhe 76133, Germany

[a)] **Author to whom correspondence should be addressed:** fei.wang@kit.edu

ABSTRACT

The size dependence of the equilibrium contact angle of sessile droplets, commonly termed line tension, lies beyond classic Young's law. Here, we identify a fundamental contribution to line tension arising from body gravity effects and surface-pressure effects within an adsorption layer. This mechanism resolves the multiscale behavior of droplets from nanometric to millimetric sizes, for which the apparent line tension changes sign and spans several orders of magnitude, consistent with existing experiments and simulations. The sign and magnitude are governed by surface wettability, the surface composition in the adsorption layer, and droplet size. Our results provide a unified physical interpretation of the experimentally observed variability in both the sign and magnitude of line tensions.

I. INTRODUCTION

It has been established through extensive experimental studies over the past decades that the equilibrium contact angle depends on droplet size. This phenomenon cannot be explained within the framework of original Young's law,[1] thereby necessitating the introduction of line tension and modified Young's law. Line tension has been observed to not be a constant material parameter[2–6] but instead to span several orders of magnitude,[7,8] while oddly exhibiting both positive and negative signs in experimental and simulation results.[6]

The sign and magnitude of line tension are of particular relevance in the design and analysis of systems, such as microfluidic devices, dropwise condensation[9] for heat transfer,[7,9] and heterogeneous nucleation.[10,11] Despite extensive investigations into the physical origins of line tension, significant disagreement persists between existing theories and the line tension measured in experiments and simulations. A consensus on the physical origins underlying various signs and magnitudes of the measured line tension has, therefore, not yet been reached.

Existing theories include distinct physical effects that are significant across different droplet sizes. At sub-nanometer atomic scales, line tension is attributed to poorly quantified direct atomic interactions.[2] At nanometric scales, the potential energy resulting from the attractive atomic forces between the liquid and the solid is modeled by the Lennard-Jones potential, with a liquid density that varies as a function of the distance from the surface, which requires a more complex numerical solution method. In the case of millimetric droplets, positive line tension becomes predominant.[2,11]

In Gibbs's theory,[12] the line tension τ is introduced directly as an independent energy contribution to the variational calculation of the system free energy F,

$$\mathrm{d}F = (\gamma_L - \gamma_G)\mathrm{d}S + \sigma \mathrm{d}A + \tau \mathrm{d}L, \tag{1}$$

where L is the length of the contact line in the sense of a sharp interface. A and S denote the areas of the liquid–gas and solid–liquid interfaces, respectively. The interfacial tensions of the liquid–gas, solid–gas, and solid–liquid phases are denoted by σ, γ_G, and γ_L, respectively.

In this work, we do not treat line tension as an independent force acting at the triple line that determines the droplet morphology. In contrast, we show that the line tension emerges as an effective quantity arising from pressure-induced variations of composition-dependent interfacial tensions within an adsorption layer. We develop a unified theory spanning six orders of magnitude

in droplet size that links line tension to surface-pressure-induced variations of composition-dependent interfacial tensions within the adsorption layer.[13,14] The theory establishes a direct connection between line tension and contact-angle hysteresis on both smooth and rough substrates.[15–17] We demonstrate that two metastable adsorption states determine the sign and magnitude of the apparent line tension. When coupled with gravitational effects, the framework predicts both the sign and magnitude of line tension as functions of droplet size and surface wettability.

II. THEORETICAL FRAMEWORK

A. Motivation of the adsorption layer

Johannes Diderik van der Waals[18] introduced the concept of a diffuse liquid–gas interface, characterized by a continuous variation in density across the interface between the liquid and gas phases. In the classical picture of Young's law, the solid–liquid and solid–gas interfaces were assumed to be sharp. Inspired by the van der Waals' considerations, we extend this concept by introducing a layer at the solid–liquid and solid–gas interfaces within which the volume fractions—and, consequently, the interfacial tensions—are varied. In our model, the adsorption layer is not treated as a continuously varying diffuse interface but as a finite interfacial region characterized by its average volume fractions. These volume fractions may differ from the corresponding bulk values and lead to modified interfacial tensions.

The concept of the adsorption layer is consistent with Cahn's theory[19,20] and a variety of simulations.[21–24]

Experimental evidence for interfacial adsorption has additionally been reported in the form of microscopic adsorbed films.[25] In MD simulations,[6,26–29] a deviation in density near the solid surface compared to the bulk can be observed. This supports the concept of an adsorption layer whose composition differs from that of the bulk.

In electrowetting, the electric field and the associated charge distribution are not strictly confined to the wetted area but extend into the surrounding solid–gas interface,[30] thereby modifying interfacial energies over a finite spatial range. This demonstrates that interfacial properties can be influenced beyond the macroscopic contact area, supporting the introduction of a spatially extended interaction region in the present model.

B. Model description

We consider a sessile droplet of volume V on an ideally smooth and chemically homogeneous substrate, forming an apparent contact angle θ and a base radius r [Fig. 1(a)]. According to Young's law,[1] the equilibrium contact angle θ_0 satisfies $\cos\theta_0 = (\gamma_G - \gamma_L)/\sigma$. In contrast, the modified Young's equation[31] incorporates corrections to the apparent contact angle that depend on the droplet size,

$$\cos\,\theta = \cos\theta_0 - \frac{\tau}{\sigma r}. \tag{2}$$

This framework captures the radius dependence of the interfacial tensions arising from pressure differences and thereby gives rise to line tension.

In contrast to the common assumption of constant fluid–solid interfacial tensions, we treat $\gamma_L = \gamma(\phi_{L1}, \phi_{G1})$ and $\gamma_G = \gamma(\phi_{L2}, \phi_{G2})$

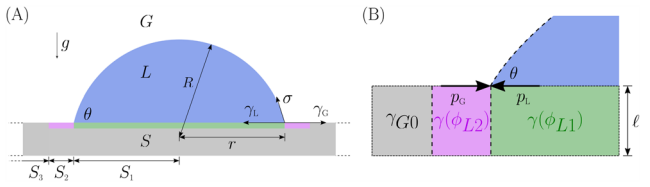

FIG. 1. (a) Schematic cross-sectional representation of the liquid droplet (L, blue) on a solid substrate (S, gray) in a gas phase (G, white). The colored layer represents the adsorption layer on the solid surface, which modifies the interfacial tensions. The wetted area, the proximal droplet penetration area, and the exterior solid–gas interfacial area are represented by S_1, S_2, and S_3, respectively. (b) Enlarged view at the triple line and the adsorption layer of thickness ℓ showing the liquid surface composition ϕ_{L1} and ϕ_{L2} dependent interfacial tensions $\gamma(\phi_{L1})$ (green) and $\gamma(\phi_{L2})$ (pink) in the vicinity of the droplet, which are affected by the liquid pressure p_L and the gas pressure p_G, respectively. Outside the proximal penetration area, the solid–gas interfacial tension γ_{G0} is considered to be constant (gray).

as functions of the average volume fractions of the liquid and gas species $\phi_{Li} = S_i^{-1}\int_{S_i}\phi_{L,\mathrm{loc}}(\vec{x})\mathrm{d}S_i$ and $\phi_{Gi} = S_i^{-1}\int_{S_i}\phi_{G,\mathrm{loc}}(\vec{x})\mathrm{d}S_i$ $(i = 1, 2)$ within the adsorption layer over the wetted area S_1 and the proximal penetration area S_2 [Fig. 1(b)], respectively. The local volume fractions of the liquid and gas species within the adsorption layer of thickness ℓ are denoted by $\phi_{L,\mathrm{loc}}(\vec{x})$ and $\phi_{G,\mathrm{loc}}(\vec{x})$, respectively. In the exterior region S_3, the solid–gas interfacial tension γ_{G0} is assumed to be constant. In our model, the volume constraint of the adsorption layer V_{ads} is enforced by the additional term pV_{ads}, where the Lagrange multiplier p represents the pressure within the adsorption layer.[32] The fluid–solid interfacial tension is modeled as

$$\gamma(\phi_L, \phi_G) = \ell[\varepsilon(\phi_L, \phi_G) + p(\phi_L, \phi_G) + \chi(\phi_L, \phi_G)]. \tag{3}$$

Here, ε, p, and χ denote the internal energy, pressure, and van der Waals energy contributions, respectively (see Appendix A).

In accordance with the constraint of the volume fractions, namely, $\phi_{L1} + \phi_{G1} = 1$ and $\phi_{L2} + \phi_{G2} = 1$, it can be concluded that only one independent variable remains. Consequently, the following simplified notation is employed: $\gamma_L = \gamma(\phi_{L1}) = \gamma(\phi_{L1}, 1 - \phi_{L1})$ and $\gamma_G = \gamma(\phi_{L2}) = \gamma(\phi_{L2}, 1 - \phi_{L2})$.

The total free energy of the system is given by

$$E = \sigma A - \Delta\gamma S_1 + \gamma(\phi_{L2})(S_1 + S_2) + \gamma_{G0}S_3 + E_g. \tag{4}$$

Here, the first three terms represent the interfacial energies, E_g denotes the gravitational body energy, and A is the area of the droplet cap. The difference in interfacial tensions is given by $\Delta\gamma = \gamma_G - \gamma_L$.

In this work, we use the spherical cap model for simplicity. For millimetric droplets, the Bond number is of order unity; consequently, the ellipsoidal cap model would provide a more accurate representation of the droplet shape here[13,48,49] but is not considered in the present study.

In the spherical cap model, the interfacial areas make Eq. (4) to

$$E(\theta, R(\theta), \Delta\gamma) = \sigma 2\pi R(\theta)^2(1 - \cos\,\theta) - \Delta\gamma\pi R(\theta)^2\sin^2\theta + E_g(\theta), \tag{5}$$

with $E_g(\theta) = \Delta\rho g V\bar{z}(\theta)$ and where R, g, and $\bar{z}$ denote the radius of the spherical cap, the gravitational acceleration, and the height

of the droplet centroid relative to the solid substrate, respectively. The density difference between the liquid and gas phases is denoted by $\Delta\rho$.

We use the Young–Laplace equation to relate the pressure of the liquid phase p_L to that of the gas phase p_G,

$$p_L = p_G + \frac{2\sigma}{R}. \tag{6}$$

The pressure difference influence $p_L - p_G$ alters the composition of the adsorption layer, thereby inducing a size dependence of the surface tension and a corresponding modification of the energy function. By defining $\Delta\gamma_0(\phi_{L1},\phi_{L2}) := \gamma_0(\phi_{L2}) - \gamma_0(\phi_{L1})$, we obtain a size-dependent expression,

$$\Delta\gamma(\phi_{L1},\phi_{L2}) = \Delta\gamma_0(\phi_{L1},\phi_{L2}) + 2\ell\Delta\phi\sigma/R, \tag{7}$$

where $\Delta\phi = \phi_{L2} - \phi_{L1}$. The intrinsic part $\gamma_0(\phi_L, 1-\phi_L)$ includes all terms in Eq. (3) except the pressure term, leading to a reference Young's contact angle $\cos\theta_0 = [\gamma_0(\phi_{L2}) - \gamma_0(\phi_{L1})]/\sigma$, which is size independent. The second term in Eq. (7) captures the surface-pressure-induced correction to the solid–fluid interfacial tension, which is the key finding of this work and leads to a size-dependent shift in the equilibrium contact angle. The balance of the surface pressure with the surface-composition-induced chemical force is supported by the Gibbs–Duhem relation in the adsorption layer.

We identify the local energy minima[15,50] of $E(\phi_{L1},\phi_{L2})$ at θ minimizing the energy at each point, as defined by Eq. (5), over the domain $\Omega := \{(\phi_{L1},\phi_{L2}) | 0 \le \phi_{L1} \le 1, 0 \le \phi_{L2} \le 1\}$ [Fig. 3(a)]. We refer to the local energy minimum at

$$\phi_{L2}^{CB} = 1 \text{ and } \phi_{L1}^{CB} = 0 \tag{8}$$

as the micro–Cassie–Baxter state (CB), in which no liquid penetrates into the adsorption layer beneath the droplet. There is a second local energy minimum, the micro–Wenzel state (W), located at

$$\phi_{L2}^{W} = 0 \text{ and } \phi_{L1}^{W} = 1, \tag{9}$$

where no gas penetrates into the adsorption layer beneath the liquid droplet. Here, the material parameters are fixed by Young's contact angle,

$$\cos\theta_{0,CB/W} = \mp\frac{\ell}{\sigma}(\Delta\varepsilon - \Delta\chi). \tag{10}$$

The remaining local energy minima at $(\phi_{L1},\phi_{L2}) = (0,0)$ and $(\phi_{L1},\phi_{L2}) = (1,1)$ correspond to states with $\Delta\phi = 0$ and, thus, exhibit no pressure-induced line tension. They are, therefore, excluded from the following analysis. The coexistence of two metastable minima separated by an energy barrier directly results in contact angle hysteresis, even on ideally smooth substrates.

By applying the volume constraint

$$R(\theta) = \left[\frac{3V}{\pi(1-\cos\theta)^2(2+\cos\theta)}\right]^{\frac{1}{3}} \tag{11}$$

to Eq. (7), we obtain $\Delta\gamma$ that depends explicitly on θ and V. This dependence leads to a modified energy function and a modified energy-minimizing contact angle, resulting in line tension. Young's law is no longer applicable to these contact angles, as the additional term in Eq. (7) depends on θ. Here, the surface pressure not only acts as a global effect but also induces a localized response within the adsorption layer.

Substituting Eq. (7) and the volume constraint Eq. (11) into Eq. (5) and minimizing the energy $E(\theta)$ yield

$$\cos\theta_0 = c - \frac{\ell\Delta\phi}{R(\theta)}(-c^2 - 2c + 1) - \frac{\Delta\rho g}{6\sigma}R(\theta)^2(1-c)^2, \tag{12}$$

with $c = \cos\theta$, which is solved for θ at each droplet size. From this procedure, we obtain $\cos\theta$ as a function of $1/r$, a relationship that is frequently observed to deviate from linearity over several orders of magnitude in droplet size in experimental studies.[2,27,40,41,47,51] As a result, the apparent line tension is typically determined *a posteriori* by the local slope, $\tau = -\sigma\frac{\mathrm{d}\cos\theta}{\mathrm{d}(1/r)}$ based on numerically solving Eq. (12).

C. Replication of Young's law and modified Young's law

The existing theories of Young's law and modified Young's law can be recovered as limiting cases of the proposed theory, demonstrating that the present framework remains consistent with established equations. First, we assume solid–liquid and solid–gas interfacial tensions $\gamma_0(\phi_{L1})$ and $\gamma_0(\phi_{L2})$, respectively, that are independent of droplet size and contact angle and do not include the pressure effect in the adsorption layer. The interfacial energy consists of contributions from the liquid–gas interface, the liquid–solid interface, and the solid–gas interface,

$$E(\theta,R,\phi_{L1},\phi_{L2}) = \sigma A_{LG} + \gamma_0(\phi_{L1})A_{SL} + \gamma_0(\phi_{L2})A_{SG}.$$

Here, $A_{LG} = 2\pi R^2(1-\cos\theta)$, $A_{SL} = \pi R^2\sin^2\theta$, and A_{SG} are the surface areas of the liquid–gas, the solid–liquid, and the solid–gas interfaces, respectively. The surface area of the solid–gas interface can be derived as the difference of total surface area of the solid surface A and the solid–liquid contact area, $A_{SG} = A - A_{SL}$. Thus, the energy function can be rearranged as follows:

$$E(\theta,R,\phi_{L1},\phi_{L2}) = \sigma A_{LG} - \Delta\gamma_0(\phi_{L1},\phi_{L2})A_{SL} + \gamma_0(\phi_{L2})A, \tag{13}$$

where $\Delta\gamma_0(\phi_{L1},\phi_{L2}) = \gamma_0(\phi_{L2}) - \gamma_0(\phi_{L1})$. We assume the last term to be constant, which has been investigated in Ref. 50, and eliminate the cap radius R by the volume constraint $V(\theta,R)$. By solving $\mathrm{d}E/\mathrm{d}\theta = 0$, we obtain Young's equation,[15,50,52]

$$\sigma\cos\theta = \Delta\gamma_0(\phi_{L1},\phi_{L2}). \tag{14}$$

In the next step, we include the line tension τ by adding $(2\pi r)\tau$ to the energy function with $r = R\sin\theta$; this size dependent energy is due to the pressure in the adsorption layer [see Eq. (7)]. First, we assume a constant line tension. The additional energy term modifies the energy minimization and leads to the modified Young's equation,[2,53]

$$\cos\theta = \frac{\Delta\gamma_0}{\sigma} - \frac{\tau}{\sigma r}. \tag{15}$$

In the present theory, the line tension is not considered to be constant, as is evidenced by experimental results. A size-dependent term is included into the interfacial tension,

$$\Delta\gamma = \Delta\gamma_0 + \Delta\gamma_1 = \Delta\gamma_0 + \frac{2\ell\Delta\phi\sigma}{R(\theta)}. \tag{16}$$

In addition, we add the body energy E_g. The minimization of the total free energy with respect to θ, under fixed droplet volume, yields Eq. (12). Here, the last two terms in Eq. (12) cause the contact angle θ to deviate from θ_0. We interpret the resulting size-dependent correction to the equilibrium contact angle as an effective line-tension contribution.

As expressed in Eq. (12), the line tension depends on θ. Equation (15) neglects the angular dependence of line tension. Iwamatsu[2] derived a generalized Young's equation that includes $\mathrm{d}\tilde{\tau}/\mathrm{d}\theta$,

$$-\Delta\gamma + \sigma\cos\theta + \frac{\tilde{\tau}}{R\sin\theta} - \frac{2+\cos\theta}{R}\frac{\mathrm{d}\tilde{\tau}}{\mathrm{d}\theta} = 0. \tag{17}$$

However, for consistent comparison with the experimental data, Eq. (15) is used to calculate the line tension. Accordingly,

$$\tau = \tilde{\tau} - \frac{2+\cos\theta}{\sin\theta}\frac{\mathrm{d}\tilde{\tau}}{\mathrm{d}\theta} \tag{18}$$

can be interpreted as an apparent line tension.

In essence, the classical theories represent limiting cases of the proposed theory. Young's law is recovered by neglecting both the body energy ($E_g = 0$) and the pressure effect within the adsorption layer ($p = 0$ or equivalently $\Delta\gamma = \Delta\gamma_0$). The modified Young's equation, Eq. (15), is obtained in a special case where the line tension is independent of the contact angle.

In the classical treatment of line tension, the solid–fluid interfacial energy difference, $\Delta\gamma_0$, is assumed to be independent of the pressure p, and the line tension effect is introduced by directly adding a size-dependent energy term, $2\pi r\tau$. In our theory, however, we do not directly introduce the size-dependent energy term $2\pi r\tau$ into the system free energy. Instead, unlike the classical approach, we assume that the solid–fluid interfacial energy difference contains an additional contribution arising from the pressure energy within the adsorption layer. By decomposing the solid–fluid interfacial energy difference into a pressure-independent term, $\Delta\gamma_0$, and a pressure-dependent term, $\Delta\gamma_1$, we obtain a modified Young's equation and the line tension energy, $\Delta\gamma_1 A_{SL} = 2\pi r\tau$. Within this framework, the pressure effect is not simultaneously incorporated into both the classical solid–fluid interfacial energy term associated with $\Delta\gamma_0$ and an independent line tension term τ.

III. RESULTS

A. Droplet size effect

Figure 2 shows the droplet size dependence of the apparent line tension at a constant Young's contact angle θ_0 as a function of the base radius for both local energy minima, obtained by varying the droplet volume. The good agreement of the theoretical curves with the experimental and simulation data points demonstrates the validity of the theory outlined above for predicting line tension. Here, the error bars indicate the range of droplet sizes over which the linear extrapolation was conducted in the respective references to calculate the line tension. Experimental measurements agree with the line tension associated with both the micro–Wenzel and micro–Cassie–Baxter states, despite the lower energy of the latter. The resulting magnitudes span from pN to μN. The magnitude of the line tension remains unaffected by the choice of adsorption layer thickness ℓ within the experimentally reported nanometer range.[54–57] The influence of different Young's contact angles on line tension is discussed below.

Figure 3(b) shows the individual contributions to the line tension as a function of the base radius, namely the surface-pressure effect and the body gravity effect. This representation reveals the droplet-size ranges in which each contribution dominates. For small droplets ($r < 3\times10^{-5}$ m), the line tension is dominated by the surface-pressure-induced contribution, while the bulk gravitational effect on the line tension is negligible. For larger droplets ($r > 10^{-4}$ m), the line tension is dominated by bulk gravity effects. An intermediate regime exhibits a continuous crossover between the two regimes. The surface-pressure-induced line tension remains approximately constant at $\sim 10^{-10}$ N for $r > 10^{-7}$ m, while the body gravitational line tension increases strongly with r.

The micro–Cassie–Baxter state and the micro–Wenzel state lead to opposite signs of $\Delta\phi$ in Eq. (7) and, thus, to opposite signs

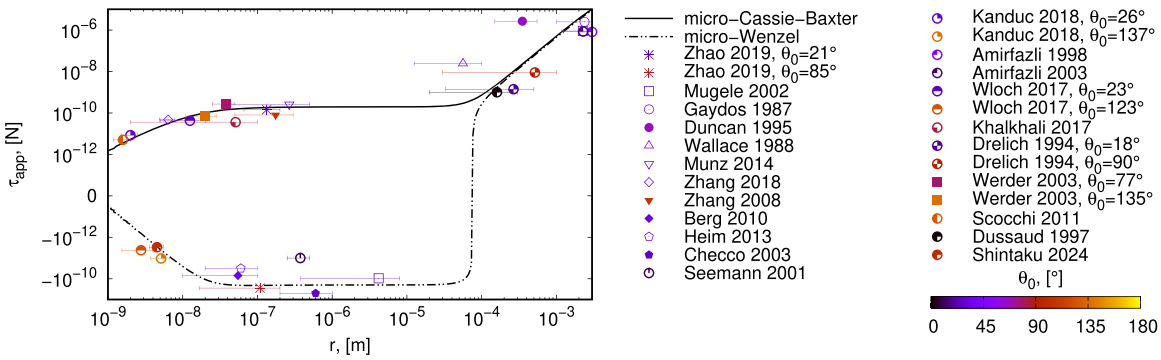

FIG. 2. Line tension τ (N) as a function of the base radius r (m) with $\theta_0 = 40°$, $\Delta\rho = 998$ kg/m^3, $g = 9.81$ m/s^2, $\sigma = 0.055$ N/m, and $\ell = 5$ nm, in comparison with previous experiments[6,10,33–46] and simulations,[3,5,26,27,29,47] where Young's contact angle, θ_0, is indicated by the color of each point.

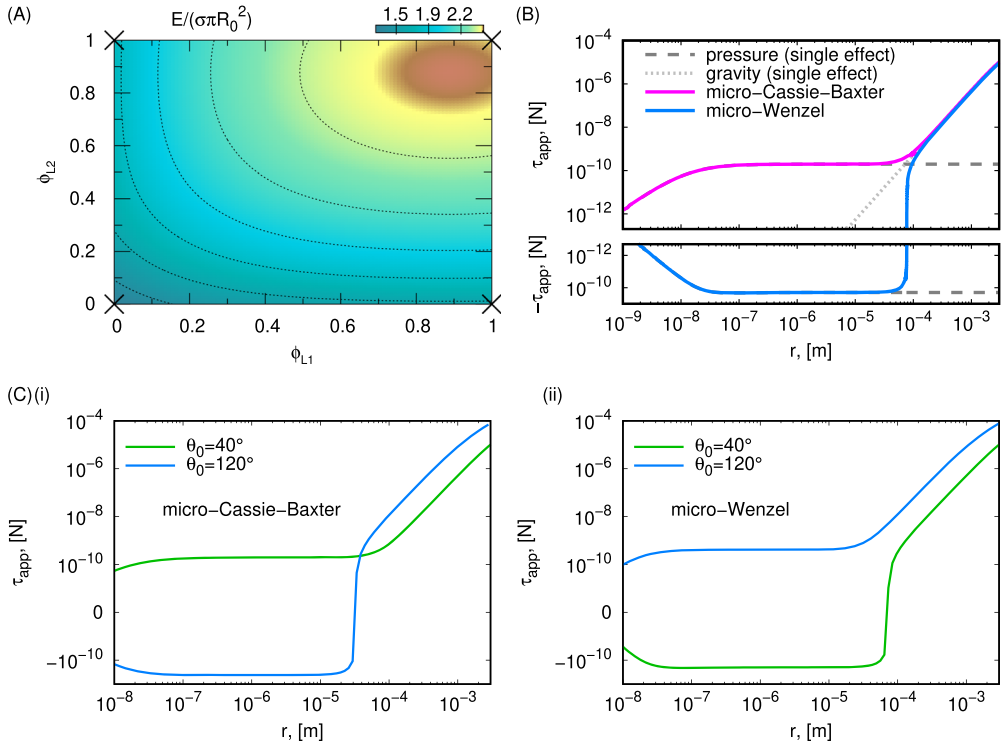

FIG. 3. (a) Energy landscape $E(\phi_{L1}, \phi_{L2})$ with local energy minima marked by crosses with an exemplary parameter: $S_2 = 0.1S_1$ (see Appendix B). (b) Line tension as a function of the base radius: single surface-pressure effect (dashed lines), single body gravity effect (dotted lines), and combined effect (solid lines; micro–Cassie–Baxter state: pink, micro–Wenzel: blue). (c) Apparent line tension as a function of the base radius for different θ_0 (different materials) at (i) micro–Cassie–Baxter state and (ii) micro–Wenzel state.

in the surface-pressure-induced line tension (positive and negative, respectively). Because the body gravitational line tension is always positive, the total line tension changes sign in the crossover regime for the micro–Wenzel state, while remaining strictly positive for the micro–Cassie–Baxter state.

Figure 3(c) shows the line tension as a function of the base radius for different Young's contact angles θ_0 at (i) the micro–Cassie–Baxter state and (ii) the micro–Wenzel state. For nanometric and micrometric droplets, the sign of the line tension depends on Young's contact angle. As illustrated in Fig. 3(c), the line tensions of the two states are either both positive or of opposite signs. In contrast, for millimeter-scale droplets, the line tension is dominated by gravitational effects and is invariably positive.

In contrast to sessile droplets, the gravitational energy contribution changes sign for pendant geometries. For larger droplets ($r > 10^{-4}$ m), where the apparent line tension is dominated by bulk gravitational contributions, this leads to a reversal in the sign of the apparent line tension.[13]

B. Origin of the sign for microscopic droplets

Having established the size dependence, the subsequent analysis focuses on the role of surface wettability. Figure 4 shows the line tension as a function of the apparent contact angle[8] at the micro–Cassie–Baxter and micro–Wenzel states, respectively. A linear regression of $\cos\theta$ as a function of $1/r$ is performed over the range of 16 nm $< r <$ 116 nm, from which the line tension is obtained as $-\sigma$ times the slope of the fitted straight line. Within the range of droplet sizes considered, Bond number is much less than 1 and gravitational effects are negligible. The micro–Cassie–Baxter state exhibits a positive line tension at small contact angles and a negative line tension at large contact angles, with a sign change at $\theta \approx 66°$, whereas the micro–Wenzel state displays the opposite behavior, with the same transition angle. The dependence of $\Delta\gamma$ on $R(\theta)$ leads to a shift in the energy-minimizing contact angle θ due to the volume constraint. Neglecting bulk energy contributions for microscopic droplets, the displacement of the equilibrium angle with respect to θ_0 follows from the equilibrium condition $\mathrm{d}E/\mathrm{d}\theta = 0$,

$$\cos\theta - \frac{\ell\Delta\phi}{R(\theta)} f(\theta) = \cos\theta_0, \tag{19}$$

with $f(\theta) = -\cos^2\theta - 2\cos\theta + 1$ resulting from the volume constraint. Equation (19) shows that sign changes in $f(\theta)$ or $\Delta\phi$ are equivalent and both reverse the line tension. Because $f(\theta)$ changes sign as θ increases, the line tension reverses accordingly. Zhao *et al.*[6] observed a sign change from positive to negative line tension at $\theta \approx 43°$. The experimentally determined magnitude of $\sim 10^{-10}$ N is in good agreement with the theoretical predictions. By comparing both local energy minima, we find that the micro–Cassie–Baxter state is energetically favored over the micro–Wenzel state for all hydrophilic

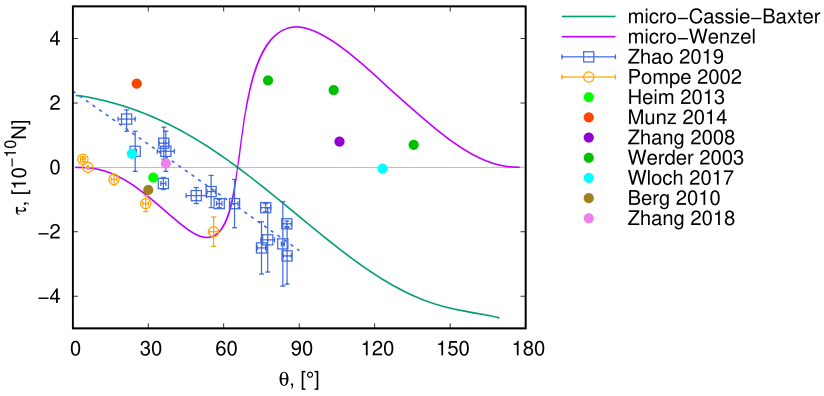

FIG. 4. Apparent line tension at the micro–Cassie–Baxter and the micro–Wenzel state as a function of the apparent contact angle θ in comparison with experimental measurements.[6,59]

contact angles. A possible cause for the deviations from the experimental data by Zhao *et al.*[6] may be the use of ionic liquids, for which electrostatic interactions[58] can contribute to both the contact angle and the line tension.

C. Macroscopic roughness effect

In the macroscopic Wenzel state,[52,58,60–62] fully wetted macroscopic surface roughness rescales the solid–liquid interfacial area in Eq. (5) by the Wenzel roughness factor f_W. Equation (19) then becomes

$$\frac{\cos\theta}{f_W} - \frac{\ell\Delta\phi}{R(\theta)} f(\theta) = \cos\theta_0. \tag{20}$$

An analogous analysis for the macroscopic Cassie–Baxter state,[52,58,60,61] with a solid fraction ψ, yields

$$\frac{\cos\theta}{\psi} - \frac{\ell\Delta\phi}{R(\theta)} f(\theta) + \frac{1-\psi}{\psi} = \cos\theta_0. \tag{21}$$

For typical roughness factors ($1 < f_W < 3$[63] and $0 \ll \psi < 1$), the macroscopic Wenzel and Cassie–Baxter states do not change the order of magnitude of the line tension. Tadmor[64,65] associated line tension with chemical and topological surface defects and the resulting contact angle hysteresis. However, the classic Wenzel and Cassie–Baxter equations alone do not show size-dependent contact angles, and no defect-induced line tensions are observed, in contrast to the experimentally observed line tension at rough surfaces of order 10^{-6} N.[66] Including the surface composition associated with the adsorption layer resolves this discrepancy. Consequently, macroscopic roughness likely contributes only a subleading effect to experimentally observed line tensions.

IV. CONCLUSION

In summary, we establish a unified and predictive theory of apparent line tension that integrates body-force effects with surface-pressure effects within an adsorption layer. The theory quantitatively reproduces experimental observations across six orders of magnitude in droplet size, including sign reversals and variations spanning several orders of magnitude—features that cannot be explained by existing mechanisms in isolation. We identify the metastable microscopic wetting state, surface wettability, and droplet size as the governing parameters controlling the sign of the apparent line tension, with droplet size additionally setting its magnitude. Distinct physical mechanisms dominate different regimes: adsorption-layer pressure effects for nanometric and micrometric droplets, and gravitational contributions for millimetric droplets. Our results demonstrate that the long-standing variability of measured line tensions reflects a systematic multiscale physical origin rather than experimental inconsistency.[7] This framework resolves a decades-old controversy and provides a unified foundation for interpreting line tension across disparate experiments and systems.

ACKNOWLEDGMENTS

F.A. thanks the Gottfried-Wilhelm Leibniz prize (Grant No. NE 822/31-1) awarded by the German Research Foundation (DFG) for funding this research. F.W. is grateful to the VirtMat project P09 of the Helmholtz Association (MSE-Programme No. 43.31.01).

AUTHOR DECLARATIONS

Conflict of Interest

The authors have no conflicts to disclose.

Author Contributions

Franziska Aurbach: Formal analysis (equal); Investigation (equal); Methodology (equal); Validation (equal); Visualization (equal); Writing – original draft (equal). **Fei Wang**: Conceptualization (lead); Methodology (equal); Supervision (lead); Validation (equal); Writing – review & editing (equal). **Britta Nestler**: Funding acquisition (lead); Project administration (lead); Writing – review & editing (equal).

DATA AVAILABILITY

The data that support the findings of this article are openly available at https://github.com/franziskaaurbach/The-microscopic-origin-of-droplet-line-tension.

APPENDIX A: INTERFACIAL TENSIONS

Our wall free energy formulation circumvents the difficulty of directly measuring the solid–fluid interfacial energies in experiments. It is constructed in analogy with the classical Gibbs free energy, $G = \varepsilon + \chi + p - Ts$, incorporating contributions from internal energy, pressure energy, and the entropic term Ts. The wall free energy has units of J/m^2, in contrast to the bulk Gibbs free energy, which has units of J/m^3. This difference in dimensionality is reconciled, within the framework of mean-field theory, by introducing an average adsorption layer thickness ℓ, which transforms the bulk free energy density into an effective surface free energy density.

The liquid–solid and solid–gas interfacial tensions consist of three terms, as follows:

$$\gamma(\phi_L, \phi_G) = \ell[\varepsilon(\phi_L, \phi_G) + p(\phi_L, \phi_G) + \chi(\phi_L, \phi_G)].$$

The volume fraction of the liquid and gas in the adsorption layer is denoted by ϕ_L and ϕ_G, respectively, with respect to which the following contributions are interpolated. The internal energy is represented by $\varepsilon = \varepsilon_L\phi_L + \varepsilon_G\phi_G$, where ε_L and ε_G are the internal energies of the liquid and gas phases, respectively. Furthermore, the van der Waals energy is denoted by $\chi = \chi_{LG}\phi_L\phi_G + \chi_{SG}\phi_G + \chi_{SL}\phi_L$, with the van der Waals interactions between the liquid–gas, solid–gas, and solid–liquid phases χ_{LG}, χ_{SG}, and χ_{SL}, respectively. The pressure term is expressed as $p = p_L\phi_L + p_G\phi_G$ and is included to ensure the volume constraint of the adsorption layer. Inserting the constraint $\phi_L + \phi_G = 1$ yields a quadratic polynomial in ϕ_L,

$$\gamma(\phi_L) = \ell\chi_{LG}\left[-\phi_L^2 + \left(1 - \frac{\Delta\varepsilon + \Delta p - \Delta\chi}{\chi_{LG}}\right)\phi_L + \xi\right],$$

with $\Delta\varepsilon = \varepsilon_G - \varepsilon_L$, $\Delta p = p_G - p_L$, $\Delta\chi = \chi_{SL} - \chi_{SG}$, and $\xi = (\varepsilon_G + p_G + \chi_{SG})/\chi_{LG}$.

Inclusion of the pressure energy in the wall free energy is essential for correctly capturing both the magnitude and the sign of the line tension. This constitutes the central contribution of the present work toward elucidating the fundamental mechanism underlying line tension.

APPENDIX B: LOCAL DROPLET PENETRATION AREA

The area S_2 describes this proximal droplet penetration area around the triple line at the solid–liquid interface. In this area, the surface composition is defined and modifies the solid–fluid interfacial tensions. It is considered to be a fraction of the wetted area S_1,

$$S_2 = \alpha S_1,$$

with $0 < \alpha \ll 1$. This factor α influences the number and location of the local energy minima of $E(\phi_{L1}, \phi_{L2})$ [see Fig. 3(a) and Ref. 50].

REFERENCES

[1] T. Young, "III. An essay on the cohesion of fluids," Philos. Trans. R. Soc. **95**, 65–87 (1805).
[2] M. Iwamatsu, "A generalized Young's equation to bridge a gap between the experimentally measured and the theoretically calculated line tensions," J. Adhes. Sci. Technol. **32**(21), 2305–2319 (2018).
[3] M. Kanduč, L. Eixeres, S. Liese, and R. R. Netz, "Generalized line tension of water nanodroplets," Phys. Rev. E **98**(3), 032804 (2018).
[4] W. Klauser, F. T. Von Kleist-Retzow, and S. Fatikow, "Line tension and drop size dependence of contact angle at the nanoscale," Nanomaterials **12**(3), 369 (2022).
[5] J. Zhang, P. Wang, M. K. Borg, J. M. Reese, and D. Wen, "A critical assessment of the line tension determined by the modified Young's equation," Phys. Fluids **30**(8), 082003 (2018).
[6] B. Zhao, S. Luo, E. Bonaccurso, G. K. Auernhammer, X. Deng, Z. Li, and L. Chen, "Resolving the apparent line tension of sessile droplets and understanding its sign change at a critical wetting angle," Phys. Rev. Lett. **123**(9), 094501 (2019).
[7] A. Amirfazli and A. W. Neumann, "Status of the three-phase line tension: A review," Adv. Colloid Interface Sci. **110**(3), 121–141 (2004).
[8] A. Marmur, "Line tension and the intrinsic contact angle in solid–liquid–fluid systems," J. Colloid Interface Sci. **186**(2), 462–466 (1997).
[9] A. Amirfazli, S. Hänig, A. Müller, and A. W. Neumann, "Measurements of line tension for solid–liquid–vapor systems using drop size dependence of contact angles and its correlation with solid–liquid interfacial tension," Langmuir **16**(4), 2024–2031 (2000).
[10] A. Amirfazli, D. Y. Kwok, J. Gaydos, and A. W. Neumann, "Line tension measurements through drop size dependence of contact angle," J. Colloid Interface Sci. **205**(1), 1–11 (1998).
[11] B. M. Law, S. P. McBride, J. Y. Wang, H. S. Wi, G. Paneru, S. Betelu, B. Ushijima, Y. Takata, B. Flanders, F. Bresme, H. Matsubara, T. Takiue, and M. Aratono, "Line tension and its influence on droplets and particles at surfaces," Prog. Surf. Sci. **92**(1), 1–39 (2017).
[12] J. Willard Gibbs, *Scientific Papers of J. Willard Gibbs, in Two Volumes: Volume 1* (Longmans, Green and Company, 1906).
[13] F. Wang, H. Zhang, and B. Nestler, "Wetting phenomena: Line tension and gravitational effect," Phys. Rev. Lett. **133**(24), 246201 (2024).
[14] H.-J. Butt, R. Berger, W. Steffen, D. Vollmer, and S. A. L. Weber, "Adaptive wetting–adaptation in wetting," Langmuir **34**(38), 11292–11304 (2018).
[15] F. Wang and B. Nestler, "Wetting and contact-angle hysteresis: Density asymmetry and van der Waals force," Phys. Rev. Lett. **132**(12), 126202 (2024).
[16] M. Preuss and H.-J. Butt, "Measuring the contact angle of individual colloidal particles," J. Colloid Interface Sci. **208**(2), 468–477 (1998).
[17] H.-J. Butt, J. Liu, K. Koynov, B. Straub, C. Hinduja, I. Roismann, R. Berger, X. Li, D. Vollmer, W. Steffen, and M. Kappl, "Contact angle hysteresis," Curr. Opin. Colloid Interface Sci. **59**, 101574 (2022).
[18] J. D. van der Waals, "The thermodynamic theory of capillarity under the hypothesis of a continuous variation of density," J. Stat. Phys. **20**(2), 200–244 (1979).
[19] J. W. Cahn, "Critical point wetting," J. Chem. Phys. **66**(8), 3667–3672 (1977).
[20] P. G. De Gennes, "Wetting: Statics and dynamics," Rev. Mod. Phys. **57**(3), 827–863 (1985).
[21] H. Zhang, H. Zhang, F. Wang, and B. Nestler, "Wetting effect induced depletion and adsorption layers: Diffuse interface perspective," ChemPhysChem **25**(14), e202400086 (2024).
[22] F. Wang and B. Nestler, "Wetting transition and phase separation on flat substrates and in porous structures," J. Chem. Phys. **154**(9), 094704 (2021).
[23] F. Wang, H. Zhang, Y. Wu, and B. Nestler, "A thermodynamically consistent diffuse interface model for the wetting phenomenon of miscible and immiscible ternary fluids," J. Fluid Mech. **970**, A17 (2023).
[24] H. Zhang, Y. Wu, F. Wang, and B. Nestler, "Effect of wall free energy formulation on the wetting phenomenon: Conservative Allen–Cahn model," J. Chem. Phys. **159**(16), 164701 (2023).
[25] D. Bonn, "Wetting transitions," Curr. Opin. Colloid Interface Sci. **6**(1), 22–27 (2001).
[26] J. Włoch, A. P. Terzyk, and P. Kowalczyk, "New forcefield for water nanodroplet on a graphene surface," Chem. Phys. Lett. **674**, 98–102 (2017).

[27]G. Scocchi, D. Sergi, C. D'Angelo, and A. Ortona, "Wetting and contact-line effects for spherical and cylindrical droplets on graphene layers: A comparative molecular-dynamics investigation," Phys. Rev. E **84**(6), 061602 (2011).
[28]S. Becker, H. M. Urbassek, M. Horsch, and H. Hasse, "Contact angle of sessile drops in Lennard–Jones systems," Langmuir **30**(45), 13606–13614 (2014).
[29]M. Shintaku, H. Oga, H. Kusudo, E. R. Smith, T. Omori, and Y. Yamaguchi, "Measuring line tension: Thermodynamic integration during detachment of a molecular dynamics droplet," J. Chem. Phys. **160**(22), 224502 (2024).
[30]H. J. J. Verheijen and M. W. J. Prins, "Reversible electrowetting and trapping of charge: Model and experiments," Langmuir **15**(20), 6616–6620 (1999).
[31]L. Boruvka and A. W. Neumann, "Generalization of the classical theory of capillarity," J. Chem. Phys. **66**(12), 5464–5476 (1977).
[32]E. M. Blokhuis, Y. Shilkrot, and B. Widom, "Young's law with gravity," Mol. Phys. **86**(4), 891–899 (1995).
[33]F. Mugele, T. Becker, R. Nikopoulos, M. Kohonen, and S. Herminghaus, "Capillarity at the nanoscale: An AFM view," J. Adhes. Sci. Technol. **16**(7), 951–964 (2002).
[34]J. Gaydos and A. W. Neumann, "The dependence of contact angles on drop size and line tension," J. Colloid Interface Sci. **120**(1), 76–86 (1987).
[35]D. Duncan, D. Li, J. Gaydos, and A. W. Neumann, "Correlation of line tension and solid–liquid interfacial tension from the measurement of drop size dependence of contact angles," J. Colloid Interface Sci. **169**(2), 256–261 (1995).
[36]J. A. Wallace and S. Schürch, "Line tension of a sessile drop on a fluid–fluid interface modified by a phospholipid monolayer," J. Colloid Interface Sci. **124**(2), 452–461 (1988).
[37]M. Munz and T. Mills, "Size dependence of shape and stiffness of single sessile oil nanodroplets as measured by atomic force microscopy," Langmuir **30**(15), 4243–4252 (2014).
[38]X. H. Zhang and W. Ducker, "Interfacial oil droplets," Langmuir **24**(1), 110–115 (2008).
[39]J. K. Berg, C. M. Weber, and H. Riegler, "Impact of negative line tension on the shape of nanometer-size sessile droplets," Phys. Rev. Lett. **105**(7), 076103 (2010).
[40]L.-O. Heim and E. Bonaccurso, "Measurement of line tension on droplets in the submicrometer range," Langmuir **29**(46), 14147–14153 (2013).
[41]A. Checco, P. Guenoun, and J. Daillant, "Nonlinear dependence of the contact angle of nanodroplets on contact line curvature," Phys. Rev. Lett. **91**(18), 186101 (2003).
[42]R. Seemann, K. Jacobs, and R. Blossey, "Polystyrene nanodroplets," J. Phys.: Condens. Matter **13**(21), 4915–4923 (2001).
[43]J. Drelich and J. D. Miller, "The effect of solid surface heterogeneity and roughness on the contact angle/drop (bubble) size relationship," J. Colloid Interface Sci. **164**(1), 252–259 (1994).
[44]T. Werder, J. H. Walther, R. L. Jaffe, T. Halicioglu, and P. Koumoutsakos, "On the water–carbon interaction for use in molecular dynamics simulations of graphite and carbon nanotubes," J. Phys. Chem. B **107**(6), 1345–1352 (2003).
[45]A. D. Dussaud and M. Vignes-Adler, "Line tension effect on alkane droplets near the wetting transition," MRS Proc. **464**, 287 (1996).
[46]A. Amirfazli, A. Keshavarz, L. Zhang, and A. W. Neumann, "Determination of line tension for systems near wetting," J. Colloid Interface Sci. **265**(1), 152–160 (2003).
[47]M. Khalkhali, N. Kazemi, H. Zhang, and Q. Liu, "Wetting at the nanoscale: A molecular dynamics study," J. Chem. Phys. **146**(11), 114704 (2017).
[48]F. Aurbach, F. Wang, and B. Nestler, "Gravitational effect on the equilibrium contact angles of sessile droplets: Theory and simulations," J. Chem. Phys. **163**(3), 034706 (2025).
[49]G. Whyman and E. Bormashenko, "Oblate spheroid model for calculation of the shape and contact angles of heavy droplets," J. Colloid Interface Sci. **331**(1), 174–177 (2009).
[50]F. Aurbach, F. Wang, and B. Nestler, "Wetting phenomena of droplets and gas bubbles: Contact angle hysteresis based on varying liquid–solid and solid–gas interfacial tensions," J. Chem. Phys. **161**(16), 164708 (2024).
[51]D. V. Tatyanenko and K. D. Apitsin, "Line tension from dual-geometry sessile droplet measurements: Combining contact-angle size-dependence data for axisymmetric and cylindrical droplets to determine the line tension," Phys. Rev. E **111**(3), 035503 (2025).
[52]W. Gene, E. Bormashenko, and T. Stein, "The rigorous derivation of Young, Cassie–Baxter and Wenzel equations and the analysis of the contact angle hysteresis phenomenon," Chem. Phys. Lett. **450**(4–6), 355–359 (2008).
[53]B. Widom, "Line tension and the shape of a sessile drop," J. Phys. Chem. **99**(9), 2803–2806 (1995).
[54]A. Méndez-Vilas, A. B. Jódar-Reyes, and M. L. González-Martín, "Ultrasmall liquid droplets on solid surfaces: Production, imaging, and relevance for current wetting research," Small **5**(12), 1366–1390 (2009).
[55]T. J. Barnes and C. A. Prestidge, "PEO-PPO-PEO block copolymers at the emulsion droplet-water interface," Langmuir **16**(9), 4116–4121 (2000).
[56]M. Heier, R. Merz, S. Becker, K. Langenbach, M. Kopnarski, and H. Hasse, "Experimental study of the influence of the adsorbate layer composition on the wetting of different substrates with water," Adsorpt. Sci. Technol. **2021**, 6663989.
[57]C. A. Prestidge, T. Barnes, and S. Simovic, "Polymer and particle adsorption at the PDMS droplet-water interface," Adv. Colloid Interface Sci. **108–109**, 105–118 (2004).
[58]H. Zhang, H. Zhang, F. Wang, and B. Nestler, "Exploration of contact angle hysteresis mechanisms: From microscopic to macroscopic," J. Chem. Phys. **161**(19), 194705 (2024).
[59]T. Pompe, "Line tension behavior of a first-order wetting system," Phys. Rev. Lett. **89**(7), 076102 (2002).
[60]E. Bormashenko, "Young, Boruvka–Neumann, Wenzel and Cassie–Baxter equations as the transversality conditions for the variational problem of wetting," Colloids Surf., A **345**(1–3), 163–165 (2009).
[61]L. Bi, F. Wang, and B. Nestler, "Wetting transition: Macroscopic roughness, static friction, and energy barrier," Phys. Rev. Res. **7**, 043093 (2025).
[62]L. Bi, F. Wang, and B. Nestler, "Surface morphology control of the Cassie–Wenzel transition: An energy landscape perspective," J. Chem. Phys. **164**(9), 094701 (2026).
[63]A. Hongru, L. Xiangqin, S. Shuyan, Z. Ying, and L. Tianqing, "Measurement of Wenzel roughness factor by laser scanning confocal microscopy," RSC Adv. **7**, 7052–7059 (2017).
[64]R. Tadmor, "Line energy and the relation between advancing, receding, and young contact angles," Langmuir **20**(18), 7659–7664 (2004).
[65]R. Tadmor, "Line energy, line tension and drop size," Surf. Sci. **602**(14), L108–L111 (2008).
[66]Z. Long, Z. Yuan, and H. Wang, "Disentangle the intrinsic line tension from the nano-corrugations induced by surface lateral roughness," Int. Commun. Heat Mass Transfer **164**, 108957 (2025).